J. Fluid Mech. (1968), *vol.* 33, *part* 4, *pp.* 673–691
Printed in Great Britain

Experimental and theoretical investigation of the stability of air flow over a water surface

By A. K. GUPTA,* M. T. LANDAHL† AND E. L. MOLLO-CHRISTENSEN
Massachusetts Institute of Technology, Cambridge, Massachusetts

(Received 26 December 1967)

An experimental investigation of the instability of a laminar air flow over water shows two distinct modes of unstable oscillations as predicted by theory. The Tollmien–Schlichting waves instability could be excited by a ribbon vibrating in the air, and the neutral stability curve determined. The water wave instability mode could be excited by a ribbon vibrating in the water. The growth rates of these waves show only fair agreement with theoretical predictions.

1. Introduction

The stability of flow over a compliant surface has received considerable attention in recent years. The interest in this subject was aroused by the work of Kramer (1960) who had observed a considerable skin friction reduction on a towed body of revolution when the body surface was covered with a flexible coating of special design. He suggested that the drag reduction was due to damping of the Tollmien–Schlichting waves because of dissipation in the flexible coating, thus causing the boundary layer to remain laminar.

Subsequent theoretical work by, among others, Benjamin (1960), Landahl (1962) and Hains & Price (1962) did, however, show that dissipation in the compliant surface actually should have a de-stabilizing effect on the Tollmien–Schlichting waves.

Benjamin (1960) found that for flow over a flexible wall there are three essentially different classes of instabilities possible, denoted by A, B and C, their occurrence depending upon surface properties and flow parameters. These instabilities in their pure forms can be identified with Tollmien–Schlichting waves (A), free surface waves (B) and Kelvin–Helmholz waves (C). Landahl (1962) was able to explain with a simple physical model why wall damping tends to destabilize class A waves, while making waves of class B more stable and leaving waves of class C relatively unaffected.

The problem of shear flow stability over a non-rigid surface is also of interest in connexion with the problem of wave generation by wind. Lock (1954) recognized that for air flow over a water surface two essentially different types of waves are possible: 'air waves' and 'water waves'. The former are the Tollmien–Schlichting waves modified by the presence of the water surface and the latter

* Present address: University of Southern California, Los Angeles, California.
† Present address: Royal Institute of Technology, Stockholm, Sweden.

correspond to Benjamin's class B in Benjamin's terminology. The growth rates of the latter have been calculated by Miles (1957, 1962).

The possibility of occurrence of Kelvin–Helmholz, or class C, instability waves was recognized already by Lamb (1932). These would appear at air speeds higher than that required for the occurrence of class A and class B waves.

An experimental verification of the theory of shear flow stability over a compliant surface requires the construction of a flexible surface of known properties. This is not an easy task, the elimination of static deflexions and prevention of reflexions of disturbances from the edges of the surface presenting difficult design problems. Despite many attempts to support a thin membrane in a wind tunnel, we did not succeed to a degree which would yield meaningful results of the kind Schubauer & Skramstad (1948) obtained in their experiments on the instability of a laminar boundary layer over a rigid surface. We therefore chose to investigate the stability of air flow over a water surface, along the lines of the previous experiments by Fischer & Blick (1966), who were primarily concerned with turbulent boundary layers.

A water surface, besides being easy to fabricate, has suitable dispersion characteristics. On the other hand, the large density ratio between water and air makes the dynamic coupling between the media small and therefore makes the interaction weak. To this is added the difficulty of controlling the physical properties of the water, surface tension in particular. In principle, the surface tension of the water can be changed by the introduction of suitable additives; this was not done in the present experiments. Thus we did not investigate the interesting problem of the effect of changes in dissipation on the growth of class A waves.

The experiments show clearly the distinction between class A and class B waves, the former being observable at low speeds over almost smooth water, and their stability boundary is only moderately modified from that of Tollmien–Schlichting waves over a rigid surface. At higher speeds, the 'water waves' (class B) appear, moving at speeds close to their free surface propagation speed. At still higher speeds, there is some evidence of Kelvin–Helmholz or class C instability.

2. Experimental arrangement

2.1. *Wind tunnel*

The wind tunnel used in the present experiment was an open circuit low turbulence tunnel with a test section cross-section of 1 ft. by 1 ft. The range of air speed was 2 ft. $\sec^{-1}$ to 30 ft. $\sec^{-1}$, the turbulence level was between 10^{-3} and 2×10^{-3}, being higher at lower air speeds. Most of the turbulent energy was in the frequency band below 10 c/s, the tunnel having a slight tendency to act as a Helmholz resonator because of its large contraction ratio (36:1). The tunnel intake was covered by 'Airmat' filter paper to avoid dust contamination of the hot wire anemometers and the water surface.

2.2. *Test section*

Figure 1 shows the test section from the side and looking downwind. After the boundary layer is removed from the lower wall, a laminar boundary layer is formed on a polished aluminum plate, 4·5 in. long and inclined at an angle of $-2{\cdot}5°$ to the free-stream direction. The water surface started at the trailing edge of the plate with a slightly convex meniscus. The water tank was 46 in. long and depth of water was 5·25 in., the depth was thus five times the longest wavelength and water depth had a negligible effect upon wave dispersion.

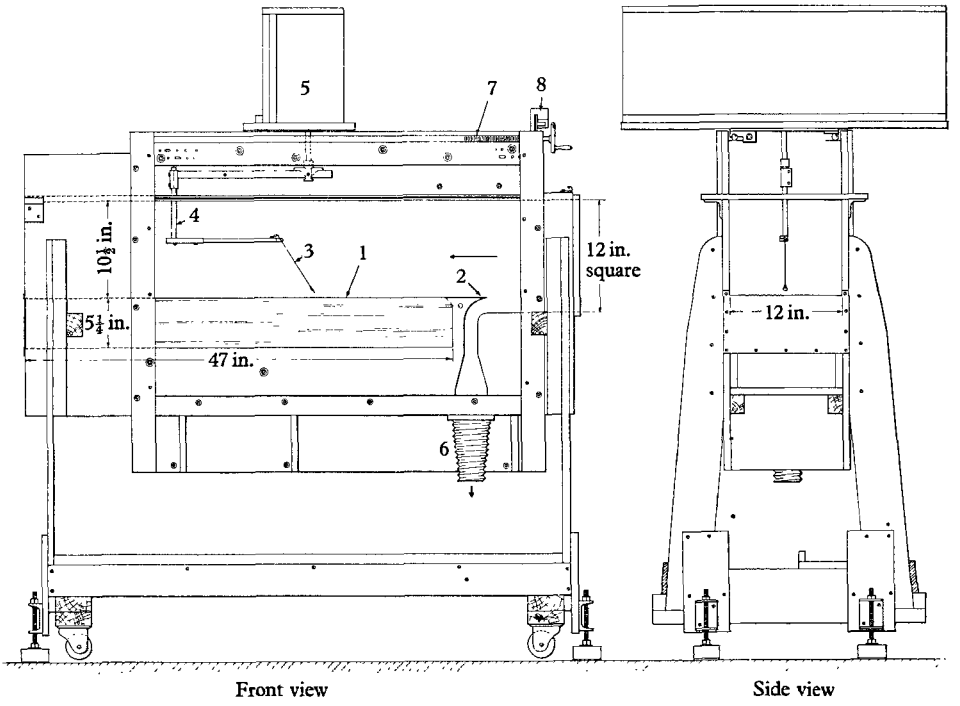

FIGURE 1. Test section (1) Water tank 46 in. × 12 in. × 5¼ in. (2) 4½ in. × 12 in. × ⅛ in. leading edge aluminium plate. (3) Probe. (4) Probe mount. (5) Vertical and spanwise traverse mechanism. (6) Hose open to atmosphere. (7) Streamwise traverse lead screw. (8) Streamwise traverse counter.

At the downstream end of the tank was another aluminum plate forming a beach of 2° inclination with the water surface.

2.3. *Hot wire anemometers and traversing mechanism*

The hot wire anemometers used were tungsten wires of 10^{-4} in. diameter, copper plate but for a $\frac{1}{16}$ in. bare section. The hot wire probes were supported on a traversing mechanism capable of positioning the wire over the full streamwise length of the test section (x) with a resolution of 10^{-2} in. and vertically (y) with a resolution of 10^{-3} in. The hot wires were used with a constant current hot wire set made by Shapiro and Edwards.

2.4. *Excitation of air and water waves*

A flat copper ribbon, 2×10^{-2} in. thick and $\frac{1}{4}$ in. wide, spanning the tunnel, was used to excite waves in the air or in the water. The ribbon was forced to vibrate by placing it in the field of a permanent magnet and passing alternating current through the ribbon. For excitation of air waves, the ribbon was placed over the aluminum plate, above the plate at $x = 3{\cdot}5$ in., measured from the plate leading edge. Only the middle 9·5 in. of the ribbon was allowed to oscillate, the ribbon being supported at the ends with cellulose tape.

For excitation of water waves, the ribbon was placed at $x = 9{\cdot}5$ in., and slightly (0·005 in.) below the water surface, forming convex menisci at the edges of the ribbon with the top dry. If the ribbon were above the water surface and with concave menisci, both air and water waves were excited and the results were difficult to interpret.

The frequency range of ribbon oscillation was 20–400 c/s for air waves and 5–50 c/s for water waves.

2.5. *Associated equipment*

The auxiliary apparatus included an electronic frequency counter for counting the shedding frequency from small cylinders for hot wire calibration, a pen recorder to record hot wire output at low frequencies, an electric stopwatch (resolution 10^{-2} sec) used to determine the speed of tracer particles in the water surface, an oscilloscope, a stroboscopic light to monitor the speed of the tunnel blower fan and a wave-form analyzer (Hewlett-Packard Model 302 A) to measure the r.m.s. values of frequency components of hot wire output above 20 c/s.

3. Experimental procedures

3.1. *Water level and compensation for evaporation*

The water was changed several times during the experiments. The equilibrium water temperature was from 3 to 5 °C below air temperature due to evaporation. The volume evaporation rate was measured at several wind speeds, using the hot wire and traverse to measure water level at several streamwise locations.

At air speeds of zero and 25·5 ft./sec, the volume rates of evaporation were 1·5 and 7·2 cm^3/min, corresponding to a rate of decrease of water level of respectively 2×10^{-4} and 10^{-3} in./min. Water was added every 10 min during the runs, a little excess water being used to maintain a convex meniscus at the upstream end of the water surface. A typical total increase in water level during a run of 5 h 10 min was 0·018 in. due to excess water addition. The 10 min interval was chosen as a compromise between the desire for constant water level and minimum water turbulence.

3.2. *Air-stream pressure gradient*

Figure 2 shows the streamwise variation of dynamic pressure $\frac{1}{2}\rho U^2$ in terms of the dynamic pressure at $x = -3{\cdot}5$ in., $x = 0$ being at the leading edge of the aluminum plate. Figure 3 shows the variation of free-stream velocity measured with a hot wire.

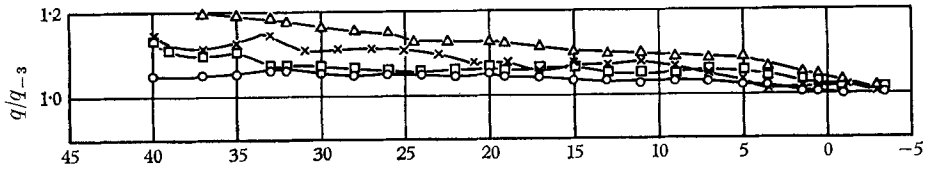

FIGURE 2. Streamwise variation of free stream dynamic pressure $q = \rho U_0^2/2$.

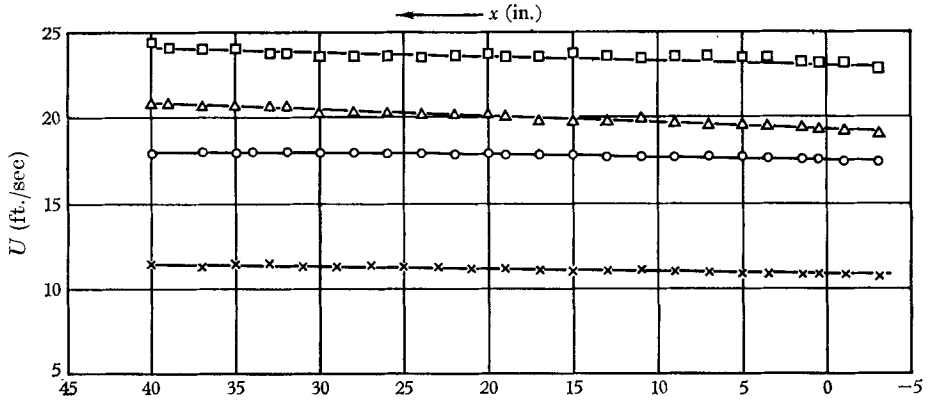

FIGURE 3. Streamwise variation of free-stream velocity U_0 at four operating air speeds.

U_0 (ft./sec.)	U_w (ft./sec.)	U_w/U_0	Values of 'x' along which U_w is measured	Pattern of surface currents
11·3	0·176	0·016	15·5 in. to 30 in. at A	
17·5	0·389	0·022	15 in. to 30 in. at B	
	0·602	0·034	5 in. to 11 in.	
20·6	0·435	0·0212	22·5 in. to 34·5 in.	
	0·626	0·0305	5 in. to 18 in.	
25·5	0·715	0·028	5 in. to 22·5 in.	
	1·02	0·04	22·5 in. to 34·5 in.	

FIGURE 4. Water current patterns.

3.3. *Water velocities*

The velocities in the water surface were measured by measuring displacements versus time of lycopodium particles sprinkled on the water surface. The patterns of particle motion were not uniform, most likely because of non-uniformities in the upstream meniscus. A typical value of water surface velocity was 3·5 % of the free-stream air speed. For cases when the lycopodium powder would be blown into patches at the downstream end ink was used to label small portions of water. The results of the two kinds of observations were in good agreement.

The observed water surface current patterns are shown in figure 4. As can be seen from the bottom sketch in figure 4, the water velocities were significant only in a thin surface layer, where they were almost one third of the phase velocity of the 'water waves' being measured. This might be significant in the comparison of our results with theory, which did not account for the presence of a non-uniform velocity field in the water.

3.4. *Measurement of spatial growth and decay of disturbances*

Oscillations were introduced in the air and in the water using the oscillating ribbon. All observations of disturbance amplitudes were made by hot wires in the air. For frequencies above 20 c/s, amplitudes were measured using a wave-form analyzer tuned to the ribbon frequency (using the constant amplitude output of the wave-form analyzer as a signal source).

For frequencies below 20 c/s, an r.m.s. meter was used, as well as a pen recorder for crude checking of the signal frequency content. Wavelengths were measured as the streamwise displacement for a phase change of 2π.

3.5. *Sources of error*

The errors in mean wind speed were below 1 %, the variations in hot wire calibration may have been as high as 10 % in the immediate vicinity of the water surface. The main source of error appears to be due to variations in water surface tension caused by contamination. The effect of this uncertainty has been largely removed by measuring the damping and dispersion of free surface waves in the tunnel. Also, during runs at higher air speeds, the contaminated surface layer was blown to the downstream end, where no measurements were made.

4. Mean boundary-layer velocity measurements

Because of our difficulties with hot wire calibration near the water surface, caused perhaps by evaporation and by local surface tension and vapour pressure anomalies near the hot wire, we show the velocity profiles obtained using a Preston tube 0·005 in. by 0·040 in. cross section. These are shown in figures 5*a*, *b* and *c*. For comparison the velocity profiles computed using the method of Lock (1954) and the profiles for an accelerating flow using Howarth's method (see Schlichting 1955) are also included.

Besides the scatter being large in the velocity profiles, the difference between experiment and theory is considerable near the water surface. We cannot account for this scattering but the following contributory reasons may be mentioned.

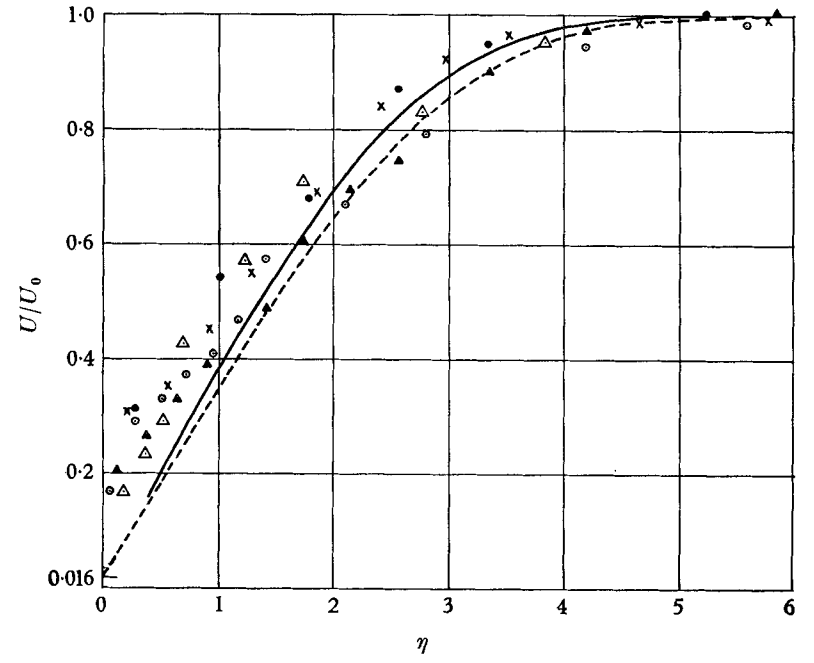

(*a*)

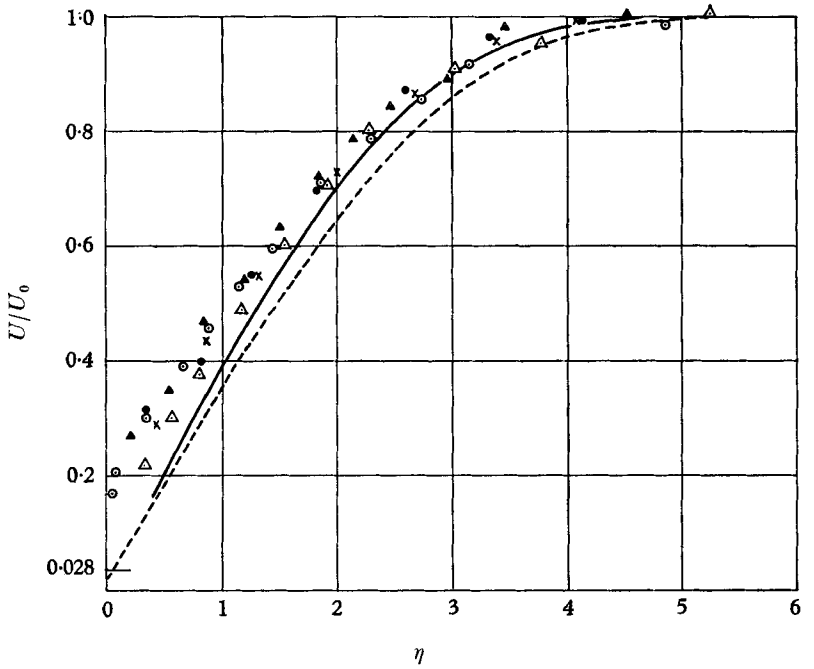

(*b*)

FIGURE 5. For legend see following page.

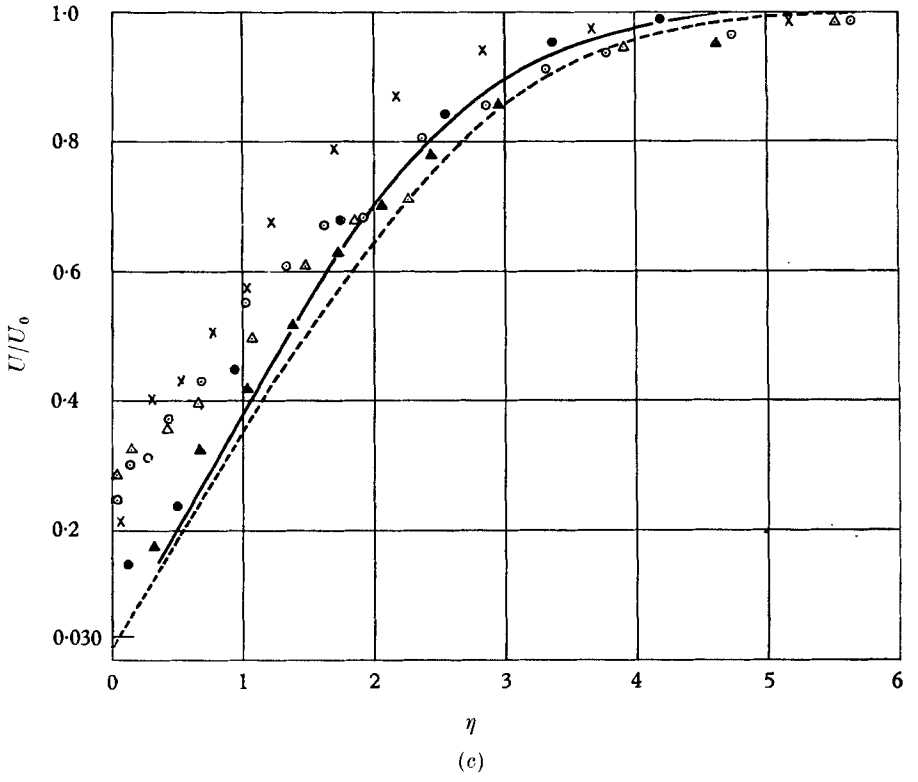

FIGURE 5. Mean velocity profiles in the boundary layer as measured with a Preston tube. Solid curve: Lock's profile for zero pressure gradient. Dashed curve: predicted by Howarth's theory with $U_0(x) = U_0(1-x^*)$ with $x^* = -0{\cdot}05$; (*a*) $U_0 = 11{\cdot}3$ ft./sec, (*b*) $U_0 = 17{\cdot}5$ ft./sec, (*c*) $U_0 = 20{\cdot}6$ ft./sec.

At the highest free-stream velocity, there were occasional bursts of turbulence observable in the hot wire traces, explaining why the velocity profiles may be transitional rather than laminar. The presence of the Preston tube near the water surface may have distorted the surface, a 'bow wave' developing, which in turn would change the velocity profile. This lack of knowledge about the mean velocity profile very near the water surface is serious when it comes to comparing theory and experiment for amplification rates of water waves (class *B*), whose speeds are less than 10 % of the free-stream velocity, and whose critical layer therefore is very close to the water surface. Finally, the Preston tube readings were not corrected for the large shear near the water surface.

5. Waves of class A

5.1. *Stability boundary*

The values for neutral stability obtained for waves excited by a ribbon vibrating in the air are shown in figures 6, 7 and 8. The neutral stability points were obtained by measuring the amplitude of velocity oscillations in the air for each frequency and airspeed as a function of streamwise distance x, and determining the

value of x and thus Re_δ for which the wave growth rate is zero. Since the presence of the water surface introduces additional dimensionless parameters, which can be expressed as Froude number and a Weber number, the neutral stability curve is different for each air speed.

The neutral curves for a laminar boundary layer over a rigid flat plate obtained by Schubaner & Skramstad (1948) are shown as dotted lines. The ordinate in

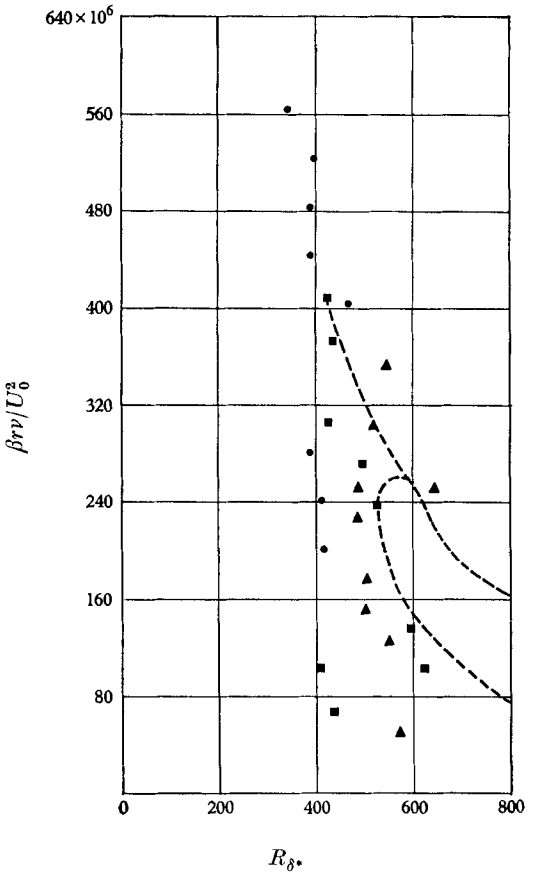

FIGURE 6. Points on the neutral stability curve $\beta_r \nu / U_0^2$ *vs.* R_{δ^*}.

figure 6 is the dimensionless frequency $\beta_r \nu / U_0$, the ordinate in figure 7 is the dimensionless wave-number $\alpha\delta$, and the ordinate in figure 8 is the real part of the dimensionless phase speed c_r / U_0. c_r is the real part of the phase speed, β_r the real part of the frequency.

The values of $Re = U_0\delta/\nu$ at the trailing edge of the plate were 269·5, 342 and 372 for the three free-stream velocities. The range of values of Re_δ which could be investigated was limited either by the instability occurring over the aluminum plate or, to attain the same Reynolds number at the ribbon position at lower speed, the ribbon would have to be moved out over the water surface, where it would catch on the surface and emit water waves.

5.2. *Velocity fluctuation amplitudes*

The hot wire output traces, shown in figure 9, show a phase reversal of u' at a certain value of y. The upper trace of each pair is the hot wire output, the lower trace of each pair the ribbon excitation signal. The upper hot wire traces have

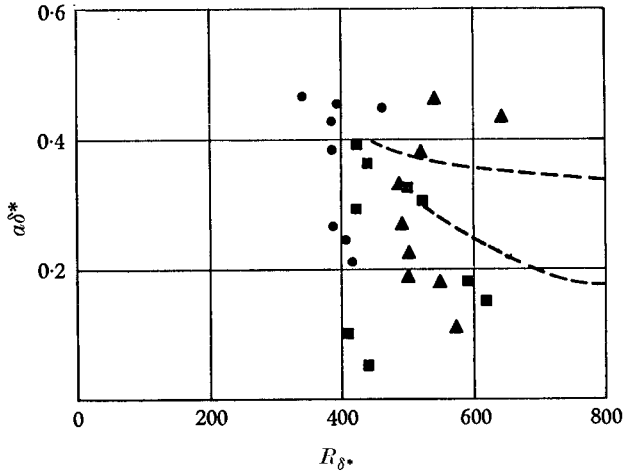

FIGURE 7. Points on the neutral stability curve in terms of $\alpha\delta^*$ *vs.* R_{δ^*}.

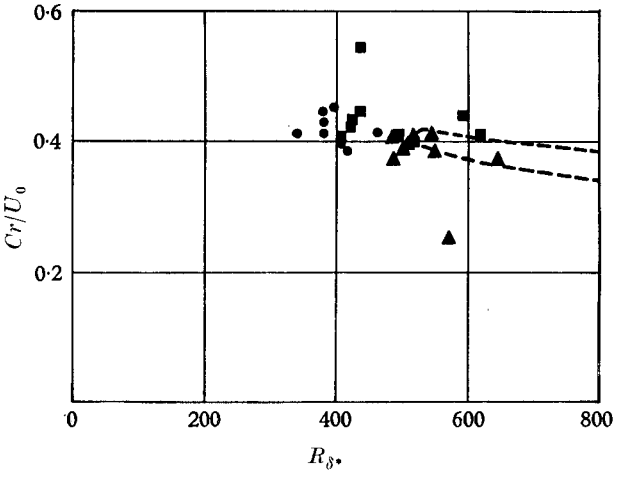

FIGURE 8. Points on the neutral stability curve in terms of c_r/U_0 *vs.* R_{δ^*}. ●, U_0 = 11·3 ft./sec; ■, U_0 = 17·5 ft./sec; ▲, U_0 = 20·6 ft./sec; Schubauer & Skramstad's (1948) results for rigid surface.

been attenuated as indicated. Figure 10 shows the amplitude distribution of u'/U_0 across the boundary layer *vs.* y/δ. In making y non-dimensional, the boundary-layer thickness δ computed assuming zero pressure gradient has been used. Since u' does not vanish at the water surface, although it must be very small, and because we could not measure u' at $y = 0$, no values are indicated for u' at $y = 0$.

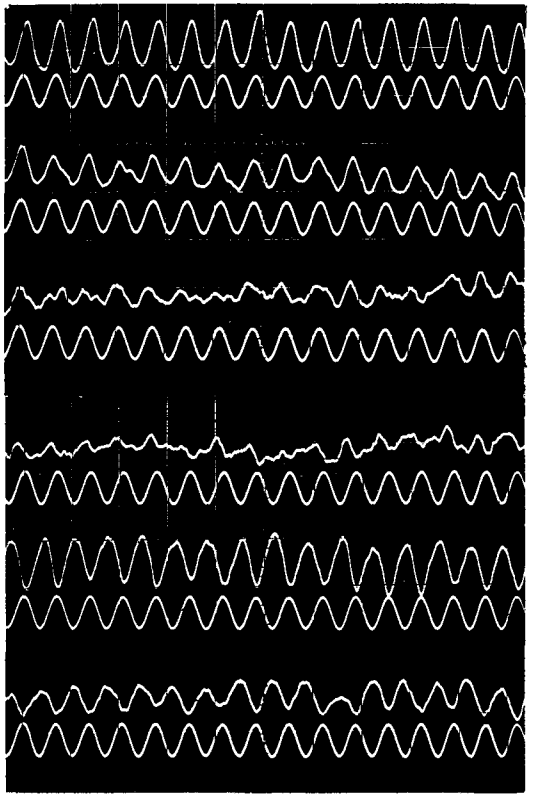

y	Att.	u'/U_0%
0·012 in.	21	0·905
0·032 in.	12	0·406
0·062 in.	0	0·067
0·072 in.	0	0·0608
0·122 in.	0	0·33
0·282 in.	0	0·18

FIGURE 9. Hot wire signal from class A waves, showing phase reversal across the critical layer. Lower trace in each pair is ribbon excitation signal.

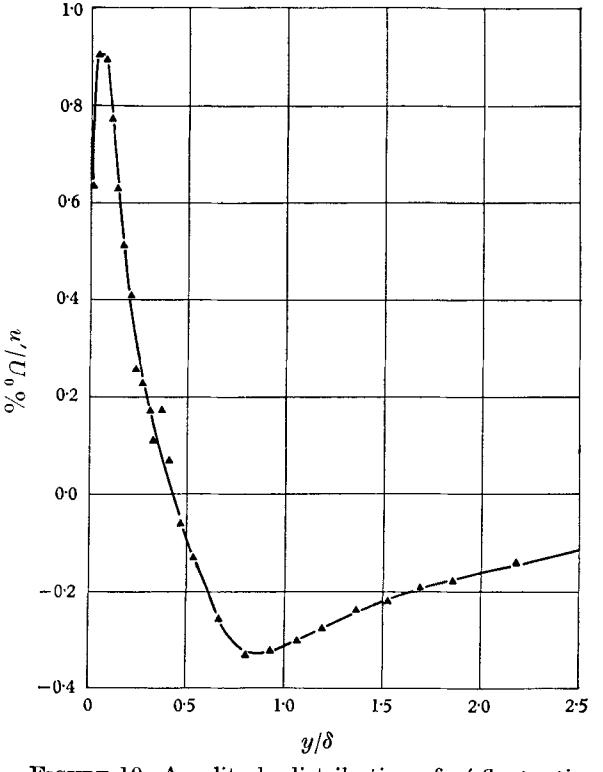

FIGURE 10. Amplitude distribution of u' fluctuations u'/U_0 *vs.* y/δ.

It should also be remarked that while water surface waves were visible at the downstream end of the tank at the higher speeds, the water surface appeared to be smooth over the range of x included in the hot wire measurements.

One qualitative observation which may have interesting implication was also made, namely, that at speeds above the critical speed for class A waves, with the ribbon stationary and no surface waves visible in the tank, if the ribbon was set into oscillation to excite class A waves at a frequency typically of 140 c/s, water surface waves at a typical frequency of between 10 and 20 c/s would occur. Turning off the ribbon excitations would make the surface waves disappear. Although this phenomenon was not investigated further, it suggests that the vorticity exchange in Lighthill's (1962) elucidation of the analysis of Miles (1962) may be significantly enhanced by the presence of an increased amplitude of class A disturbances, which may provide for more intensive diffusion of oscillatory vorticity across the critical layer. This supposition must of course be investigated more systematically in a suitably designed experiment.

6. Stability of waves of class B

Class B disturbances, which are primarily water surface waves, were excited by a vibrating ribbon in the water surface. As judged from the hot wire output, the excitation caused water waves to appear at lower air speeds than when no excitation was present. This was really a consequence of the low level of turbulence and ambient vibration level in the tunnel. At high air speeds the waves at the downstream end of the test section were only weakly dependent on excitation. The waves which were observed at air speeds below 21 ft./sec were two-dimensional; i.e. 'long crested', while the waves occurring above 21 ft./sec were three-dimensional or 'short crested'.

At a given air speed, the higher the excitation frequency, the weaker the wave growth. The maximum wave amplitude observed was 0·04 in. and occurred at 6 c/s and $U_0 = 20{\cdot}6$ ft./sec, this wave amplitude measured in wavelengths was 0·022 or, in terms of trough to crest height, 0·044 wavelengths.

The spatial decay or growth of the waves was measured using a hot wire to observe streamwise velocity fluctuations in the air. Figure 11 shows some typical traces, suggesting how well the amplitude may be measured using an r.m.s. meter. Figures 12 *a*, *b*, *c* and *d* show the logarithm or r.m.s. wave amplitude *vs.* downstream distance at several frequencies for $U_0 = 0$, 11·3, 17·5 and 22·6 ft./sec, respectively.

As can be seen, the first wave growth occurs at 11·5 ft./sec for waves of frequency 5 c/s. The scatter in figure 12 is probably the effect of repeated additions of water to compensate for evaporation. The reversal of the amplitudes for 15 and 20 c/s waves at $U_0 = 20{\cdot}6$ ft./sec is within the range of experimental error.

The measured dispersion relationships between wave length and phase speed are shown in figure 13 for several air speeds. The highest and lowest phase speeds measured were $0{\cdot}0995U_0$ and $0{\cdot}467U_0$, respectively, this is from two to four times the observed speed for the water surface layer. The dotted curve is the theoretical

dispersion relationship for water at rest: $c^2 = (g/\alpha) + (T\alpha/\rho)$ where $\alpha = 2\pi/\lambda$ is the wave-number and T is the surface tension. The differences between experimental and theoretical phase speeds at zero air speed for small wavelengths were most likely due to the higher surface tension caused by the contamination of the

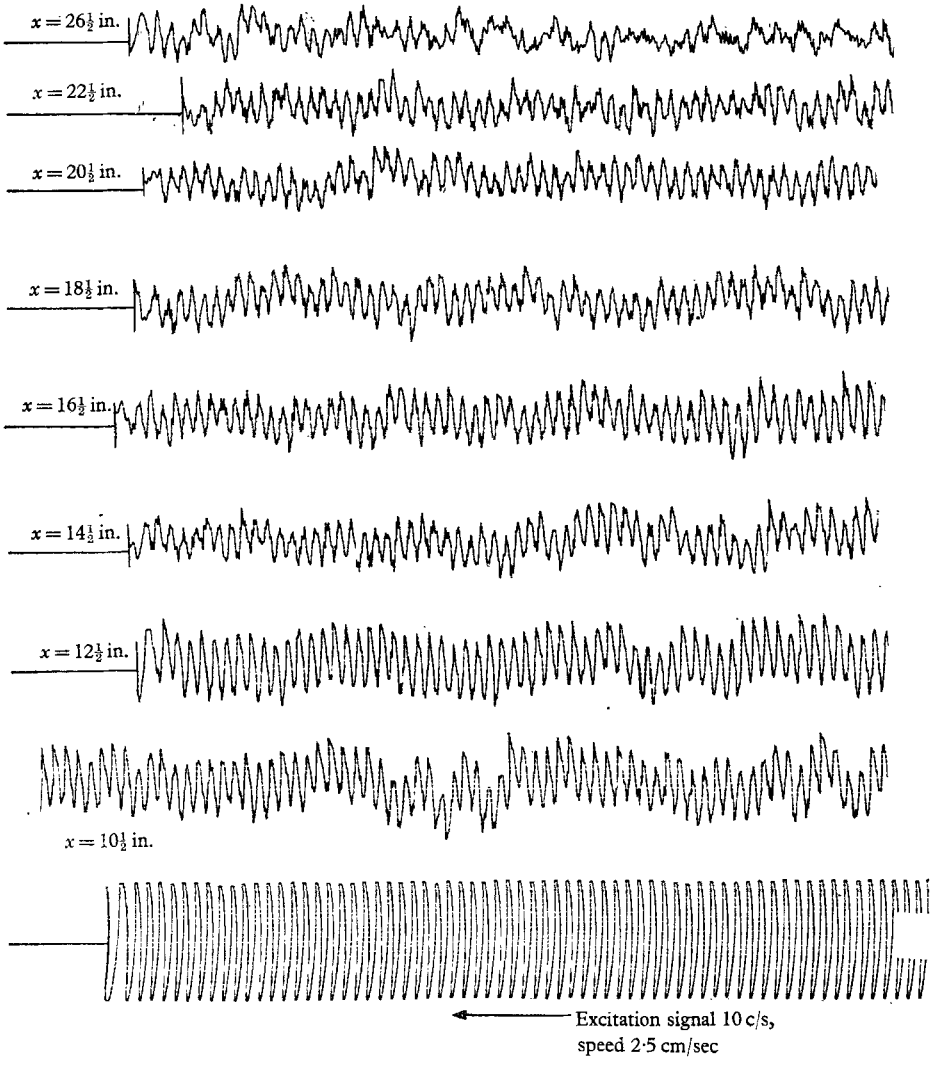

FIGURE 11. Streamwise velocity fluctuations over class B waves for $U_0 = 17{\cdot}5$ ft./sec at an excitation frequency of 10 c/s.

water surface. The higher phase speeds observed with the air moving are in part due to the water surface currents, and in part due to the changes in phase speed caused by the instability phenomenon under investigation.

The spatial amplification rates were found from figure 12 which shows that the amplitude of u' varies exponentially with distance.

By setting $u'(x,t) = \hat{u}\exp(i\alpha x - \omega t) = \hat{u}\exp\{-\alpha_i x + i\alpha_r(x - c_r t)\}$ one may obtain from figure 12 the e-folding distance of amplitude.

In order to interpret this information in terms of temporal growth of a wave with purely real wave-number, which is the formulation used in theoretical treatments of stability, we use the results obtained by Gaster (1962) which show that the temporal growth rate for purely real wave-number is $\zeta = \alpha_r c_i = -\alpha_i c_g$ where c_g is the group velocity.

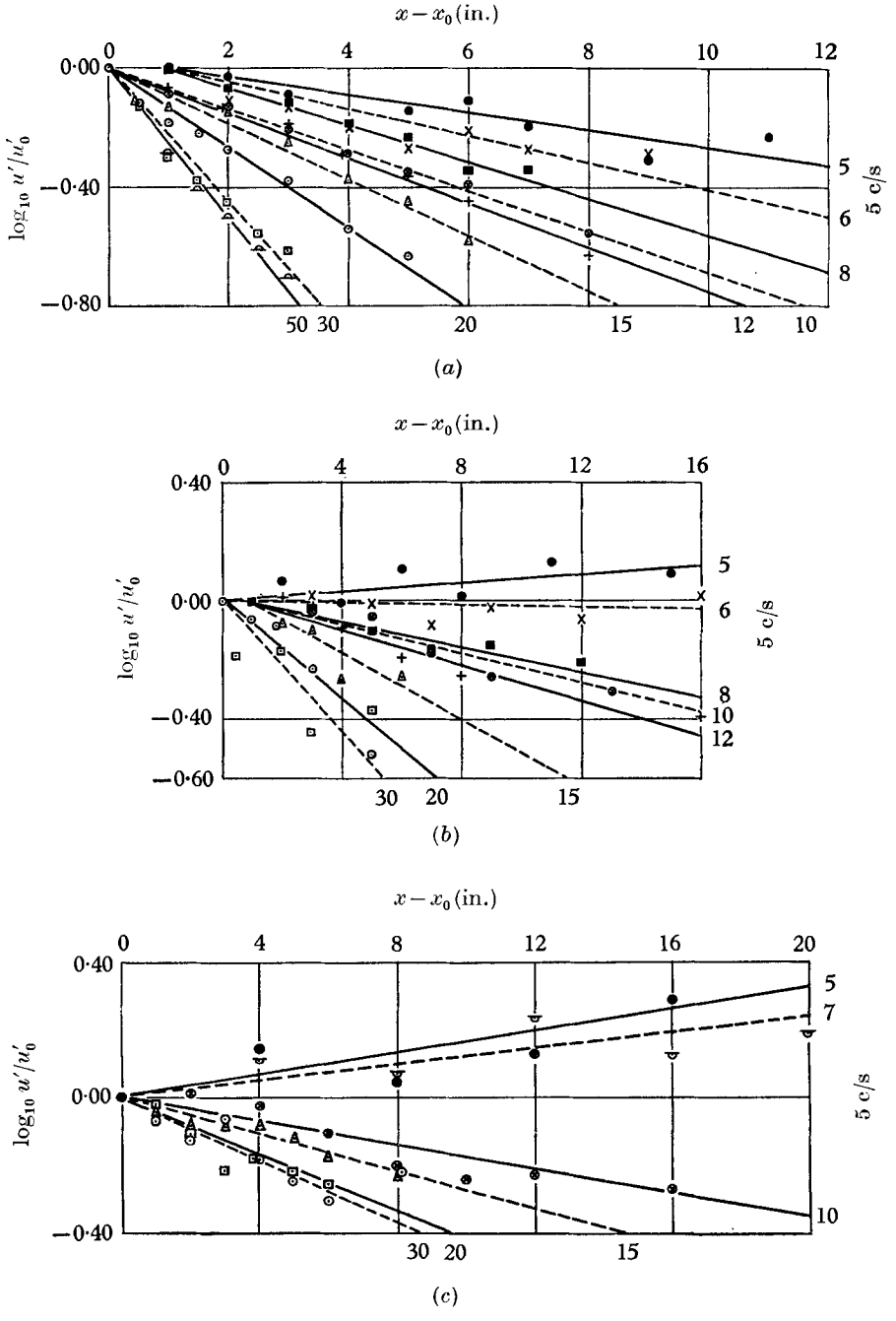

FIGURE 12. For legend see p. 15.

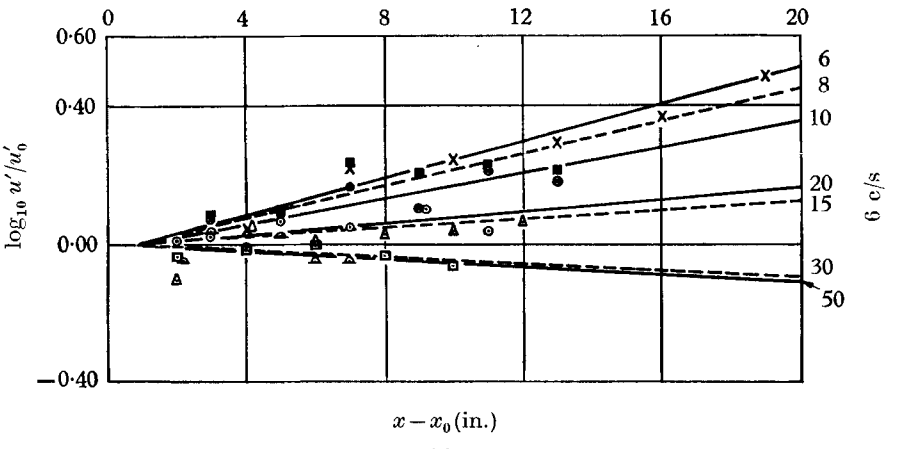

FIGURE 12. Root-mean-square u' amplitude *vs.* downstream distance x with wave generator frequency as parameter for different airspeeds U_0.

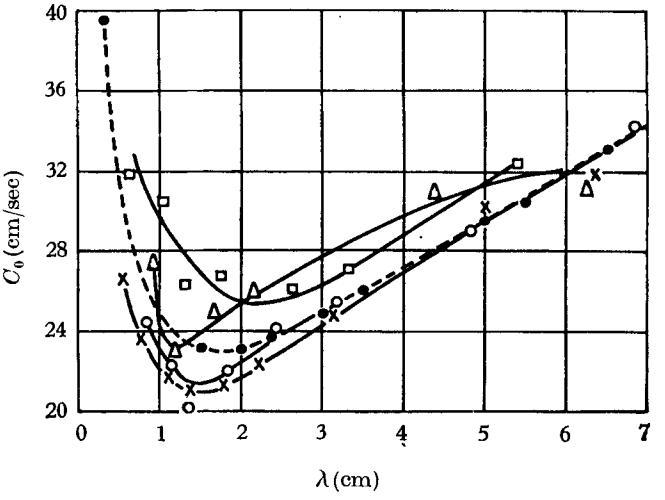

FIGURE 13. Measured results for phase speed c_r *vs.* wavelength. Dashed curve; theoretical relation for $U_0 = 0$.

For zero air speed, the theoretical temporal decay rate is $\zeta w = -2\alpha^2 \nu_w$; ν_w is the kinematic viscosity of water. The theoretical values of phase and group velocity are respectively: $c = (g/\alpha + T\alpha/\rho)^2$ and $c_g = (c^2 + wT\alpha/\rho)/2c$. If ζ is the observed amplification rate and $-\zeta_w$ the observed damping rate at zero air speed, we may attribute the difference to the effect of wind, and define the amplification rate due to wind as: $\zeta_a = \zeta + \zeta_w$. The measured and theoretical water damping rates are shown in figure 14.

Figure 15*a*, 15*b* and 15*c* show the values ζ_a obtained from the experiments and, for comparison, the results of computer solutions for theoretical growth rates using the program system developed by Landahl (1966). Two sets of theoretical amplification rates are shown, based on different air-velocity profiles.

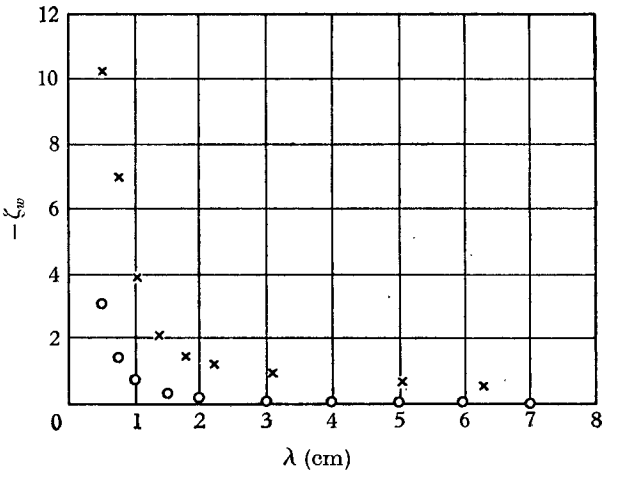

FIGURE 14. Measured values of wave damping $-\zeta_w$, ×, observed; ○, theoretical.

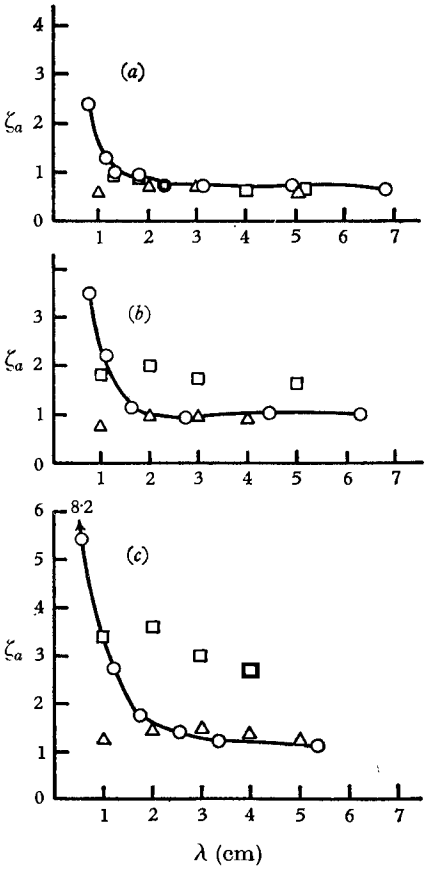

FIGURE 15. Wave amplification rate $\zeta_a = \zeta + \zeta_w$ after taking account of viscous dissipation in the water. (*a*) $U_0 = 11{\cdot}3$ ft./sec, (*b*) $U_0 = 17{\cdot}5$ ft./sec, (*c*) $U_0 = 20{\cdot}6$ ft./sec. ○, measured; △, calculated using Lock's theoretical velocity profile; □, calculated using a least mean-squares fit to velocity profiles measured with hot wires.

The points shown as squares are based on a least-square polynomial fit to the velocity profiles obtained by hot wire measurements. The triangles are based on velocity profiles calculated from Lock's theory. The experimental points are indicated by circles.

The theoretical values assume zero water velocity, a surface tension equal to that of pure water and the dynamic boundary condition at the water surface

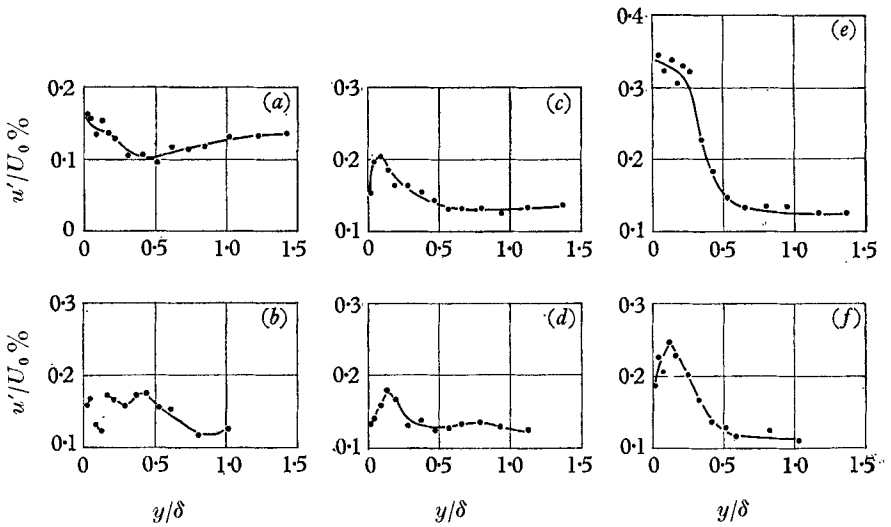

FIGURE 16. Amplitude of velocity fluctuations over class B waves *vs.* y/δ for several excitation frequencies and air speeds.

U_0(ft./sec)	f(c/s)	U_0(ft./sec)	f(c/s)
(*a*) 11·3	6	(*d*) 17·5	10
(*b*) 11·3	10	(*e*) 20·6	6
(*c*) 17·5	7	(*f*) 20·6	10

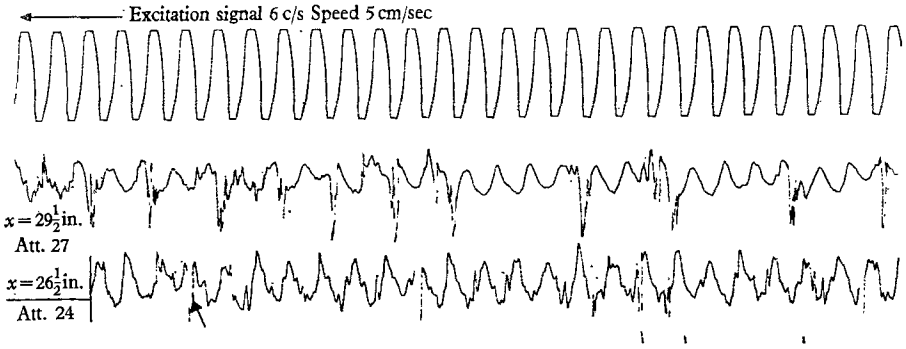

FIGURE 17. Velocity fluctuations over class B waves showing bursts of turbulence. U_0 = 20·6 ft./sec, y = 0·040 in., x = 26·5 in. (lower trace) and 29·5 in. (middle trace).

includes the inviscid response of the water to pressure both in normal and tangential velocities.

The calculated results do not show the large increase in amplification rate at small wavelengths that was observed experimentally.

The main inaccuracy in the theoretical results stems from the uncertainties in the velocity profiles used in the calculations. The measured velocity profiles show considerable scatter, and since the crucial feature of the velocity profile is its curvature $d^2U(y)/dy^2$ near the critical layer, which for water waves is very near the water surface, it appears that the weakest point in the comparison between the experiment and theory is in experimental error in velocity profile measurements very near the water surface. It was also established by numerical experimentation that the calculated growth rate was rather sensitive to the assumed velocity profile, in particular those variations which involved a substantial change in profile curvature near the water surface.

Another cause of discrepancy between theory and experiment was the difference in surface tension between low and high air speeds. In the latter case, the contaminated surface layer was swept downstream, leaving the area where observations were made largely uncontaminated.

A possible source of error in the calculations is the neglect of mean velocity shear in the water. In fact, the measured velocity fluctuations show that for the most strongly amplified wavelengths the maximum streamwise velocity amplitude occurs at the point nearest the water surface, suggesting that the critical layer may be in or below the water surface. This unlikely possibility is of course theoretically possible.

Examples of measured streamwise velocity fluctuation u'/U_0 amplitudes as functions of height above the water surface y are shown in figure 16. The maximum amplitude is close to the water surface as expected, and the curves are reminiscent of those obtained by Kaplan (1964) for the instability of flow over a membrane.

Figure 17 shows recorder traces of u' *vs.* time, and the first occurrence of bursts of turbulence can be seen. The intermittency of turbulent bursts may be due to subharmonic wave frequency content, although more careful experiments will be needed to ascertain this.

7. Conclusions

The instability of laminar air flow over water occurs in two modes, as predicted by theory. The class A mode of disturbances are the Tollmien–Schlichting waves as modified by the presence of the water surface. The general shape of the neutral stability curves is preserved, but shows a clear dependence upon dimensionless parameters introduced by the water surface, namely Froude and Weber numbers.

Class B waves are shown to have growth rates in crude agreement with linear theory.

This work was supported by the Office of Naval Research under Nonr 1841(74) and by the Air Force Office of Scientific Research under AF 49-638-1493.

REFERENCES

BENJAMIN, T. B. 1960 *J. Fluid Mech.* **9**, 513.

FISHER, D. H. & BLICK, E. B. 1966 *J. Aircraft*, **3**, 163.

GASTER, M. 1962 *J. Fluid Mech.* **14**, 222.

HAINS, F. D. & PRICE, J. F. 1962 *Phys. Fluids*, **5**, 365.

KAPLAN, R. E. 1964 *The Stability of Laminar Incompressible Boundary Layers in the Presence of Compliant Boundaries.* ASRL TR116-1, MIT.

KRAMER, M. O. 1960 *J. Aero. Sci.* **27**, 68.

LAMB, H. 1932 *Hydrodynamics.* New York: Dover.

LANDAHL, M. T. 1962 *J. Fluid Mech.* **13**, 609.

LANDAHL, M. T. 1966 *A Time-Shared Program System for the Solution of the Stability Problem for Parallel Flows over Rigid or Plane Surfaces.* MIT ASRL Rept. 116-4.

LIGHTHILL, M. J. 1962 *J. Fluid Mech.* **14**, 3, 385–398.

LOCK, R. C. 1951 *Quart. J. Mech. Appl. Math.* **4**, 42.

LOCK, R. C. 1954 *Proc. Camb. Phil. Soc.* **50**, 105.

MILES, J. W. 1957 *J. Fluid Mech.* **3**, 185.

MILES, J. W. 1962 *J. Fluid Mech.* **13**, 433.

SCHLICHTING, H. 1955 *Boundary Layer Theory.* New York: Pergammon Press.

SCHUBAUER, G. B. & SKRAMSTAD, H. K. 1948 *NACA Rept.* no. 909.